

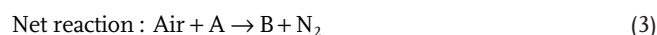
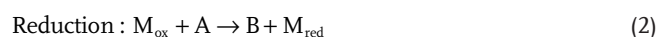
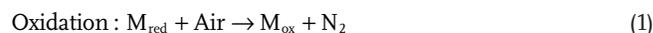
High-Throughput Analysis of Materials for Chemical Looping Processes

Nicholas R. Singstock, Christopher J. Bartel, Aaron M. Holder,*
and Charles B. Musgrave*

Chemical looping is a promising approach for improving the energy efficiency of many industrial chemical processes. However, a major limitation of modern chemical looping technologies is the lack of suitable active materials to mediate the involved subreactions. Identification of suitable materials has been historically limited by the scarcity of high-temperature (>600 °C) thermochemical data to evaluate candidate materials. An accurate thermodynamic approach is demonstrated here to rapidly identify active materials which is applicable to a wide variety of chemical looping chemistries. Application of this analysis to chemical looping combustion correctly classifies 17/17 experimentally studied redox materials by their viability and identifies over 1300 promising yet previously unstudied active materials. This approach is further demonstrated by analyzing redox pairs for mediating a novel chemical looping process for producing pure SO₂ from raw sulfur and air which could provide a more efficient and lower emission route to sulfuric acid. 12 promising redox materials for this process are identified, two of which are supported by previous experimental studies of their individual oxidation and reduction reactions. This approach provides the necessary foundation for connecting process design with high-throughput material discovery to accelerate the innovation and development of a wide range of chemical looping technologies.

1. Introduction

Chemical looping processes are a promising route for improving energy efficiency,^[1–4] leveraging renewable energy sources,^[5–11] facilitating chemical conversions,^[12–20] and reducing undesirable emissions across many sectors of the chemical industry.^[21–26] The most common chemical looping (CL) processes involve an oxidation reaction (Equation (3)) that is separated into two subreactions, mediated by the redox chemistry of a “looped” active material.^[27–29] In the oxidation subreaction (Equation (1)), oxygen from air is transferred to an oxygen-deficient active material (M_{red}) to generate the oxidized active material (M_{ox}). M_{ox} is then reduced by reactant A to form product(s), B, to regenerate the reduced form of the active material, M_{red} (Equation (2)). This division of a single reaction (Figure 1a; Equation (3)) into multiple subreactions via a CL scheme (Figure 1b; Equations (1) and (2)) can decrease or eliminate the need for downstream separations to isolate product(s) B,^[23,29,30] improve the exergy efficiency of the process,^[29,31,32] and overcome thermodynamic limitations imposed by operating at a single temperature^[15,27,33]



Chemical looping combustion (CLC) and chemical looping reforming are two chemical looping processes that may provide an energy-efficient solution to CO₂ capture and syngas production, respectively, and are therefore of considerable interest to the utilities sector.^[23,29,31,34,35] Other applications that leverage CL have been examined for the production of high purity, value-added chemicals such as hydrogen,^[33,36,37] oxygen from noncryogenic separation of air,^[38,39] hydrocarbons,^[15,17,40,41] and ammonia.^[5,12,42] A more general CL scheme applicable to all of these processes is provided in Section S1 (Supporting Information). Despite promising results from pilot-scale studies and techno-economic analyses for many

N. R. Singstock, Prof. A. M. Holder, Prof. C. B. Musgrave
Department of Chemical and Biological Engineering
University of Colorado
Boulder, CO 80309, USA
E-mail: aaron.holder@colorado.edu; charles.musgrave@colorado.edu

Prof. C. J. Bartel
Department of Materials Science and Engineering
University of California
Berkeley, CA 94720, USA

Prof. A. M. Holder, Prof. C. B. Musgrave
National Renewable Energy Laboratory
Golden, CO 80401, USA

Prof. C. B. Musgrave
Department of Chemistry
University of Colorado
Boulder, CO 80309, USA

Prof. C. B. Musgrave
Renewable and Sustainable Energy Institute
University of Colorado
Boulder, CO 80309, USA

 The ORCID identification number(s) for the author(s) of this article can be found under <https://doi.org/10.1002/aenm.202000685>.

DOI: 10.1002/aenm.202000685

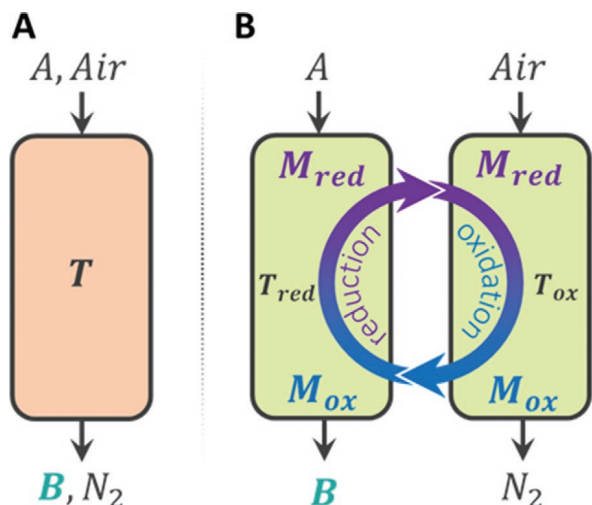


Figure 1. A) A single-step oxidation reaction operating at temperature T , Equation (3). B) The same overall reaction as in (A) reconceived as a two-step chemical looping cycle mediated by a looped active material M_{ox}/M_{red} . In the oxidation reactor (right), M_{red} is oxidized to M_{ox} by air. N_2 (and any unreacted O_2) is removed as an effluent. M_{ox} is reduced by A in a separate reactor, producing product B (undiluted) and regenerating M_{red} . Equations (1)–(3) provide the detailed reactions.

of these CL processes,^[43–47] the realization of industrial-scale units has encountered substantial challenges.^[29,48–51] The primary barrier to commercialization of CL technologies is the lack of suitable active materials that lead to economically viable processes.^[23,29] A superior active material should exhibit low material cost, high anion transport capacity, high reaction conversion, high recyclability, high attrition resistance, and fast reaction kinetics.^[23,29,52]

The identification of materials with superior figures of merit for CL has remained a long-standing challenge.^[29,52] Although some of these properties can be readily determined or predicted, such as the cost of a material or its theoretical anion transport capacity, most require a detailed knowledge of the thermodynamic properties of the material system. To date, the few studies that have leveraged computational tools to identify active materials for CL processes have predominantly relied on experimental data, namely, the temperature-dependent Gibbs formation energy of a material, $\Delta G_f(T)$.^[12,52–55] Knowledge of $\Delta G_f(T)$ of the candidate materials within a chemical system enables the determination of equilibrium products as a function of temperature and elemental composition, thus providing the reaction conversion and recyclability of an active material for a given CL process. Unfortunately, experimental values of $\Delta G_f(T)$ are only tabulated for a limited set of materials,^[56] and calculating $\Delta G_f(T)$ from first principles is too computationally demanding for high-throughput materials screening.^[57–59] The lack of free energy data for solid compounds limits the total number of materials that can be screened based on their thermodynamics and the extent to which they can be analyzed (e.g., the competition with side reactions). Consequently, previous studies aimed at identifying viable CL materials have evaluated only dozens of candidates.^[12,52–55]

Recently, we reported a statistically learned descriptor, $G^\delta(T)$, for calculating the formation free energies, $\Delta G_f(T)$, of

crystalline solid compounds at temperatures up to 1800 K.^[60] The descriptor $G^\delta(T)$ requires only the composition, formation enthalpy and atomic density of a material at 0 K, which are widely tabulated in open databases of density functional theory (DFT)-computed materials properties.^[60] We exploit $G^\delta(T)$ to provide the foundation for our high-throughput thermodynamic screening approach to rapidly identify active materials with high reaction conversion and high recyclability (i.e., low side product formation). Attrition resistance and reaction kinetics cannot be obtained with our high-throughput screening approach because they depend on properties beyond the free energies of the active materials, such as the support material, particle size, regeneration time, activation barriers, etc. However, these properties can nevertheless be tuned via the system parameters after viable active materials have been identified based on thermodynamic screening.^[18,25,61–63]

We previously applied a thermodynamic screening approach based on the descriptor $G^\delta(T)$ to rapidly identify active materials for solar-thermal ammonia synthesis in which ≈ 1100 oxide and nitride pairs were analyzed.^[7] Here, we demonstrate that this approach can be applied to any CL process that operates at or near equilibrium conditions with temperatures up to at least 1800 K, irrespective of the active material class (e.g., oxide, halide, etc.), the number of subreactions,^[7] or the number of reactant and/or product species. This includes well-studied CL processes (e.g., CLC,^[23] CL reforming,^[35] water splitting,^[33] etc.) and emerging applications (e.g., air separation,^[38] ammonia synthesis,^[5,12] chemical looping with oxygen uncoupling,^[64] three-way catalysis,^[24] etc.). In this work we provide a detailed assessment of the accuracy of this method, including the expected errors in predicted reaction free energies and the classification accuracy for identifying thermodynamically viable (i.e., high conversion) active materials. Based on the success of this approach in correctly classifying thermodynamically viable active materials, we applied it to discover previously unstudied active materials for CLC with high reaction conversion, high recyclability, high transport capacity, and low cost.

In addition to demonstrating our descriptor-based method for evaluating materials for CLC, we also applied it to evaluate materials for a novel process that we propose for sulfur dioxide (SO_2) production. This is a compelling process to improve with CL because SO_2 is conventionally produced via the aerobic combustion of sulfur, which yields a dilute mixture of SO_2 in air and thus requires energy intensive separations to concentrate the SO_2 and limit SO_2 emissions.^[65] We suggest a CL scheme for sulfur oxidation that yields pure SO_2 from sulfur and could provide a more energy-efficient and lower emission route to both concentrated SO_2 and sulfuric acid, the world's most produced chemical by mass.^[66] We identified 12 promising active materials for this process using our thermodynamic screening approach. Previous experimental studies of the individual oxidation and reduction reactions of a number of these materials corroborate our predictions. We expect that as the field of CL continues to grow, this robust and high-throughput screening approach based on machine-learned thermodynamic properties will provide an effective method for discovering active materials for a wide range of CL chemistries.

2. Results and Discussion

2.1. Error Quantification for Gibbs Energy of Reaction

We calculated $\Delta G_r(T)$ for 26 oxidation reactions where experimental data was available to estimate the error of our $\Delta G_r(T)$ calculations (Figure 2; Table S2, Supporting Information). The mean absolute error (MAE) in $\Delta G_r(T)$ in units of kJ mol O_2^{-1} is approximated by Equation (4) where T is the temperature in Kelvin. The absolute error for the corresponding reduction reactions are, by definition, identical to the errors for the oxidation reactions. The MAE between the experimentally obtained and computationally predicted $\Delta G_r(T)$ is comprised of two components, the 0 K contribution from the DFT-calculated enthalpies and the temperature-dependent contribution from our $G^\delta(T)$ descriptor. These errors arise exclusively from the solid-state compounds because all data for gas-phase species are experimentally determined thermochemical properties. The reaction enthalpies contribute the $42.7 \text{ kJ mol O}_2^{-1}$ error present at 0 K, and $G^\delta(T)$ contributes the temperature-dependent error, which increases approximately linearly according to $0.0108T$ (where T is in K and the error is in kJ mol O_2^{-1}). The 0 K error contribution of $42.7 \text{ kJ mol O}_2^{-1}$ agrees with our broader study of 415 decomposition reactions at 0 K which yielded an MAE of $88\text{--}100 \text{ meV atom}^{-1}$ ($\approx 51 \text{ kJ mol O}_2^{-1}$ with respect to these 26 reactions).^[67] This error was shown to vary only moderately across many material classes (e.g., oxides, halides, pnictides, etc.)^[67]

$$\Delta G_r(T) : \text{MAE}(T) = 42.7 + 0.0108 T \quad (4)$$

Furthermore, the temperature-dependent error contribution of $0.0108T$ ($19 \text{ kJ mol O}_2^{-1}$ at 1800 K), which arises exclusively from errors in $G^\delta(T)$, agrees with the previously reported MAE of 46 meV atom^{-1} ($\approx 25 \text{ kJ mol O}_2^{-1}$ with respect to these 26 reactions) for $G^\delta(T)$ applied to 178 test compounds.^[60] The root mean squared error of 61 meV atom^{-1} for these 178 compounds differs only moderately from the MAE, which indicates that the error arising from $G^\delta(T)$ varies only slightly across the many diverse material classes studied (e.g.,

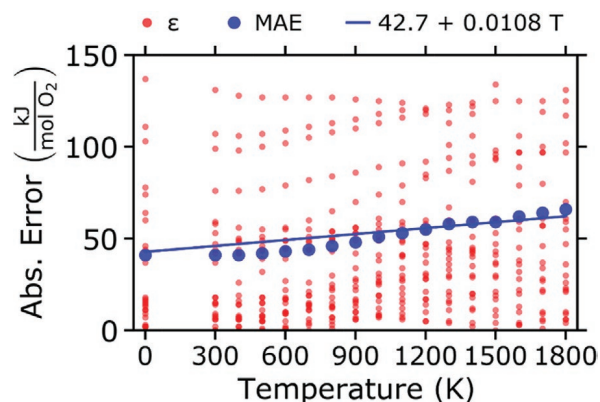


Figure 2. Absolute error (ϵ) of experimental versus predicted $\Delta G_r(T)$ for 26 oxidation reactions as a function of temperature (red). The mean absolute error (MAE) at each temperature assessed is shown in blue. $R^2 = 0.84$ for the linear regression model of MAE ($\text{MAE} = 42.7 + 0.0108T$).

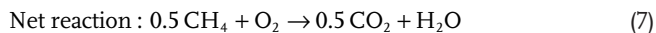
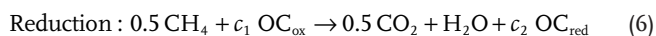
alkalis, transition metals, halides, etc.).^[60] The temperature-dependent component of the error determined here for $\Delta G_r(T)$ is lower than the respective error previously calculated for individual materials, suggesting that a favorable cancellation of errors exists between similar materials for redox reactions (e.g., Fe_3O_4 to Fe_2O_3). Additionally, because neither of the two contributing factors to the error in $\Delta G_r(T)$ vary substantially by material class, the error in $\Delta G_r(T)$ will also not vary substantially by material class. Consequently, these results indicate that our thermodynamic screening approach can be applied with similar accuracy to any chemical looping process that operates near equilibrium for both the oxidation and reduction reactions, irrespective of the active material chemistry. For processes like CLC where a large range ($\approx 400 \text{ kJ mol}^{-1}$) exists between the upper ($\Delta G_r = 0$) and lower ($\Delta G_r = \Delta G_{\text{net}}$) bounds on ΔG_r that bracket the oxidation reaction of the thermodynamically viable active materials, the MAE is less pronounced relative to this range than for CL processes where a narrower range of ΔG_r values are viable, such as chemical looping reforming or chemical looping air separation.

2.2. Benchmarking with Chemical Looping Combustion

Our descriptor-based thermodynamic screening approach involves 5 steps: 1) generate all possible redox pairs (i.e., pairs of anion-rich/ M_{ox} and anion-deficient/ M_{red} materials), 2) apply the $G^\delta(T)$ descriptor to obtain $\Delta G_r(T)$ for all materials, 3) calculate $\Delta G_d(T)$ (decomposition free energy, Section S3, Supporting Information) and remove redox pairs that include unstable materials, 4) calculate $\Delta G_r(T)$ for all subreactions and remove redox pairs where any subreaction (Equations (1) and (2)) is not spontaneous at the specified conversion within the temperature range of interest, and 5) perform Gibbs energy minimization over all chemical species in the chemical system for each redox pair to determine conversion and side product formation (see the Experimental Section for additional details). Properties such as material price and oxygen transport capacity (R_{OC}) were subsequently calculated for thermodynamically viable redox pairs. We used a reaction conversion of 90% as the threshold for thermodynamic viability in this study.

In order to assess the efficacy of our thermodynamic screening approach to identify thermodynamically viable redox pairs, we benchmarked it using experimentally studied oxygen carrying materials for CLC. We considered a diverse set of 10 materials with experimental reaction conversions of methane $>90\%$ and 7 materials that demonstrate low or no conversion of methane, such as support materials (Table S4, Supporting Information).^[23,62,68–75] We used the aerobic combustion of methane as the net reaction for this benchmarking study, where the oxidation and reduction reactions for this process are shown in Equations (5) and (6), respectively, and the net reaction is shown in Equation (7). Oxygen carriers (OCs) are active materials for CLC, where $\text{OC}_{\text{ox}}/\text{OC}_{\text{red}}$ is equivalent to $M_{\text{ox}}/M_{\text{red}}$ and Equations (5)–(7) are the CLC analogs of Equations (1)–(3). The stoichiometric coefficients for the oxidized and reduced phases of the OC are denoted by c_1 and c_2 , respectively. These

coefficients were normalized so that 1 mole of O_2 is liberated from OC_{ox} to react with 0.5 moles of methane



The oxidation reaction is always spontaneous because the redox pairs are only considered at temperatures where the constituent compounds are stable (i.e., OC_{ox} does not spontaneously decompose to OC_{red}). Consequently, the spontaneity of the reduction reaction (Equation (6)) determines the thermodynamic viability of candidate redox pairs for CLC. The reduction reaction is equivalent to the difference between the net reaction and the oxidation reaction (Equation (8)). Thus, if the net reaction is more exergonic than the oxidation reaction at a given temperature ($\Delta G_{r,net}(T) < \Delta G_{r,ox}(T)$), then the reduction reaction is spontaneous and the corresponding redox pair is thermodynamically viable

$$\Delta G_{r,red} = (0.5\Delta G_{f,CO_2} + \Delta G_{f,H_2O} - 0.5\Delta G_{f,CH_4}) - (c_1\Delta G_{f,OC_{ox}} - c_2\Delta G_{f,OC_{red}}) \quad \Delta G_{r,red} = \Delta G_{r,net} - \Delta G_{r,ox} \quad (8)$$

The Ellingham diagram for CLC shown in **Figure 3** provides calculated $\Delta G_{r,ox}$ as a function of temperature for the 17 experimentally studied materials. We consider the temperature range of 600–1200 °C because this is the conventional operating range for CLC.^[23] In addition to $\Delta G_{r,ox}(T)$, the net combustion reaction for CLC ($\Delta G_{r,net}$) is shown at 90% conversion of methane (black line). The 10 redox pairs that have been experimentally demonstrated to react with methane to form CO_2 and steam

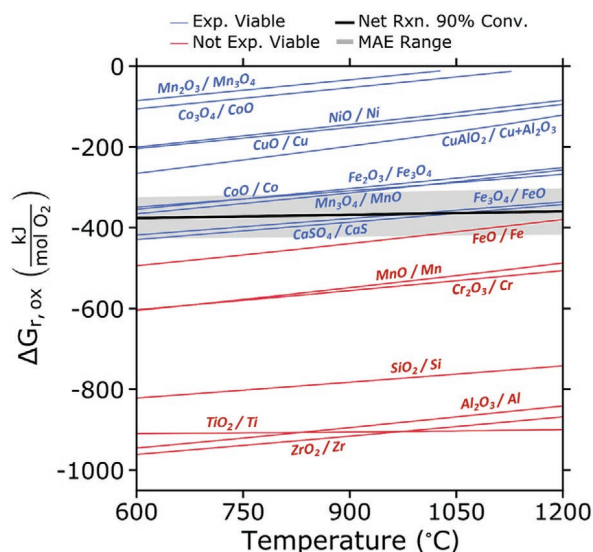


Figure 3. Ellingham diagram showing the calculated oxidation energy, $\Delta G_{r,ox}$, for the 17 experimentally studied redox pairs as a function of temperature from 600 to 1200 °C. OCs with a high experimental conversion of methane (>90%) are shown in blue, while OCs that experimentally do not react with methane or exhibit low methane conversion are shown in red. The bold line indicates the free energy of the net reaction, $\Delta G_{r,net}$, for methane oxidation at 90% conversion. Redox pairs are labeled as OC_{ox}/OC_{red} .

at >90% conversion are shown in blue, and the 7 materials that have been experimentally observed to not react with methane or which are often used as inert support materials are shown in red. We note that although $\Delta G_{r,net}$ is obtained from experiment, the MAE for $\Delta G_r(T)$ (Equation (4)) is included above and below the net reaction to indicate whether the calculated $\Delta G_{r,ox}$ values lie within the MAE range of being thermodynamically viable pairs.

Our thermodynamic screening approach correctly classifies all 10 of the experimentally studied redox pairs with >90% methane conversion for CLC (blue lines in Figure 3). These 10 pairs were predicted to be both stable and thermodynamically viable within the operating temperature range for CLC. Our method also correctly classifies all 7 redox pairs that were reported to exhibit low or no conversion of methane as not being thermodynamically viable for CLC (red lines in Figure 3). Furthermore, the prediction by our analysis that $CaSO_4/CaS$ transitions to being thermodynamically viable at higher temperatures agrees with experimental observations.^[72] The $CaSO_4/CaS$ redox pair was reported to transition from 10% conversion of methane to CO_2 at 850 °C to 90% conversion at 1000 °C, closely matching our results that this redox pair should demonstrate >90% conversion above ≈ 1050 °C.^[72] Additionally, the reduction of Fe_3O_4 to FeO was observed to be slow at 950 °C, matching our model's prediction that this redox pair has a low thermodynamic driving force (small $|\Delta G_{r,red}|$) at 950 °C despite being thermodynamically viable.^[62]

Although $\Delta G_{r,ox}$ indicates whether a given redox pair is thermodynamically capable of oxidizing methane, it does not account for the possibility of side-product formation. To address this, we performed Gibbs energy minimization on the oxidized material of each redox pair in the presence of a stoichiometric amount of methane to determine the yield of CO_2 at equilibrium considering all possible species within our database that can be formed from $M_{ox} + CH_4$. The prediction of equilibrium product yields of these 17 redox pairs further corroborated the classification results. Of the 10 OCs that have been experimentally demonstrated to be viable, all exhibit calculated CO_2 yields >97% except $CaSO_4/CaS$ and Fe_3O_4/FeO which are predicted to yield a mixture of CO , CO_2 , H_2O , and H_2 as combustion products, as is observed experimentally.^[69,76] All 7 of the redox pairs that are not experimentally viable are calculated to exhibit conversions below 1%. Overall, our high-throughput screening approach accurately classifies all 17 of the experimentally studied redox pairs by their thermodynamic viability and agrees with experimental observations for the two redox pairs that lie on the threshold of thermodynamic viability.

2.3. New Active Materials for Chemical Looping Combustion

In order to identify new redox pairs for CLC, we obtained 13 763 oxygen-containing binary and ternary compounds from MP. Of these, 3107 were predicted to be stable ($\Delta G_d(T) < 0$, see the Experimental Section) at some temperature between 300 and 1800 K using our $G^\delta(T)$ descriptor. This subset of stable compounds was used to generate 17 880 redox pairs. Of these pairs, 1320 meet the condition for thermodynamic viability ($\Delta G_{r,net}(T) < \Delta G_{r,ox}(T)$) within the CLC operating range for a methane conversion of >90%. This subset includes the 10 experimentally viable redox pairs analyzed in the previous section. **Figure 4a** depicts

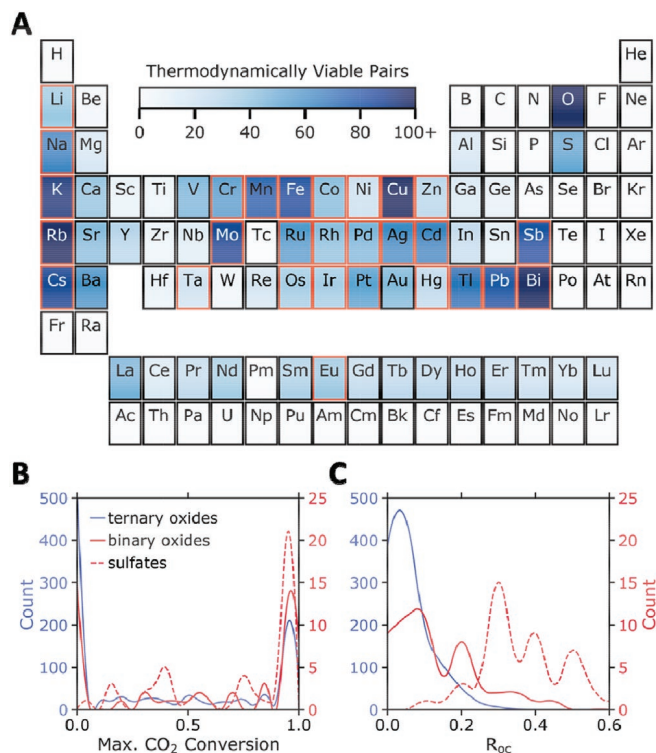


Figure 4. A) The number of thermodynamically viable redox pairs (1320 total) for CLC that contain each respective element. The 27 elements highlighted by an orange border form viable binary oxide redox pairs. B) Histogram of maximum CO₂ conversion obtained between 600 and 1200 °C for the 1320 viable redox pairs categorized by class of the oxidized OC material (ternary oxide, binary oxide, and sulfate). C) Histogram of R_{OC} values for the 1320 viable redox pairs, categorized by material class. Histograms are smoothed with an interpolation function.

the subset of elements that these 1320 redox pairs are composed from, as well as the number of predicted thermodynamically viable redox pairs containing each element. The 27 highlighted elements (orange borders) form the oxides that comprise the 52 viable binary redox pairs. In the case of ternary redox pairs, 91% of the 1268 ternary pairs that our scheme predicts are viable contain at least one of these 27 elements. The remaining 108 viable ternary compounds do not contain any of these 27 elements and thus would not have been identified by alloying a viable binary. Binary pairs of the alkali metals (Li, Na, K, Rb, Cs), some transition metals (Mo, Pd, Ag, Os, Pt), and some main group elements (Zn, Cd, Sb, Hg, Tl, Pb, and Bi) include materials with melting points below 600 °C,^[77] and Ru, Rh, and Ir are too expensive for industrial CLC applications.^[78] Excluding binary pairs composed of these elements further reduces the element set to Mn, Fe, Co, Ni, and Cu, which have all been studied as CLC OCs and are included to benchmark our method, in addition to Ta and Eu, which have not been explored for CLC. The two unstudied binary pairs are TaO₃/Ta₂O₅ and Eu₂O₃/Eu₃O₄.

TaO₃ forms in a layered structure that has been synthesized through delamination of RbTaO₃^[79] but has not been studied for high-temperature applications. In contrast, our prediction that Eu₂O₃/Eu₃O₄ is thermodynamically viable for CLC is corroborated by the synthesis of Eu₃O₄ from Eu₂O₃ and CO,^[80] demonstrating that Eu₂O₃ oxidizes CO to CO₂ and therefore likely

also oxidizes methane. Moreover, the melting point of Eu₂O₃ (2291 °C) is higher than any other material that comprises a viable binary OC for CLC,^[77] suggesting that this material may have a higher attrition resistance than other currently studied OCs. The oxidation of Eu₂O₃ to Eu₃O₄ has a similar thermodynamic driving force ($\Delta G_{r,ox}$) to that of the Fe₂O₃/Fe₃O₄ redox pair which exhibits fast reaction kinetics and full methane conversion.^[62] Although Eu₂O₃/Eu₃O₄ has a low R_{OC} of 0.02, it is similar to that of Fe₂O₃/Fe₃O₄ (0.03).^[69] While Gibbs energy minimization predicts that competing formation of EuCO₃ will lower methane conversion to CO₂, this could be overcome at higher temperature (>1200 °C). Furthermore, the cost of Eu₂O₃ is greater than that of other currently studied OCs.^[78] Nonetheless, Eu₂O₃/Eu₃O₄ is an intriguing candidate for CLC at temperatures near or above 1200 °C.

Gibbs energy minimization was performed on the 1320 thermodynamically viable redox pairs in order to determine the conversion of methane to CO₂ and the yields of the desired OC materials for the oxidation and reduction reactions, with consideration of possible competing phases (i.e., side products). Figure 4b shows the maximum CO₂ conversion calculated between 600 and 1200 °C for each redox pair, which exhibits a bimodal distribution with peaks near 0% and 100% CO₂ conversion. The majority of redox pairs either suffer from side product formation and thus yield minimal or no CO₂ in the reduction reaction, or minimal side product formation occurs and full conversion to CO₂ is observed. Calculated R_{OC} values for the 1320 thermodynamically viable redox pairs are provided in Figure 4c, categorized by the oxidized material class. High R_{OC} pairs are those with a large difference in the mass of oxygen between the oxidized and reduced phases, making them more efficient CL materials. Sulfate pairs (i.e., sulfate/sulfide) exhibit the highest average R_{OC} values and constitute 60% of the pairs with $R_{OC} > 0.25$ due to the high oxygen content of the sulfate anion which liberates two moles of O₂ when fully reduced to the sulfide. The oxide pairs with R_{OC} values near or above 0.25 predominantly contain elements as the reduced phase, limiting the number of pairs meeting this constraint.

343 redox pairs are predicted to convert methane to CO₂ with >90% conversion, and 315 of these exhibit a conversion >95%. Of these 315, 152 also yield the desired oxidized and reduced phase(s) with a conversion >95% for the oxidation and reduction reactions, respectively. Of these 152 redox pairs, 13 also exhibit a $R_{OC} > 0.05$ and a price under \$20 kg⁻¹, making them exceptional candidates for CLC. 4 of these 13 pairs are comprised of known materials included in our benchmarking (CuO/Cu, NiO/Ni, CuAlO₂/Cu+Al₂O₃, and Mn₃O₄/MnO). The remaining 9 pairs of this set (Bi₂(SO₄)₃/Bi₂S₃, CuSO₄/CuS, MnO₂/Mn₂O₃, Sb₂(SO₄)₃/Sb₂S₃, ZnSO₄/ZnS, Cu₂SO₅/Cu₂S, CdSO₄/CdS, PbSO₄/PbS, and CrCuO₂/Cr₂O₃ + Cu) are discussed in detail in the following paragraph. 165 other redox pairs meet these R_{OC} and price requirements but exhibit a conversion < 95% for at least one of the reactions. However, it is important to note that the Gibbs energy minimization scheme is more sensitive to ΔG_f than the thermodynamic viability assessment, and consequently small errors in ΔG_f can potentially produce substantial errors in predicted reaction conversions. This is because a small shift in ΔG_f could stabilize or destabilize a material relative to competing phases, resulting in a substantial change in the equilibrium products.

Table 1. Select redox pairs for CLC with oxidation and reduction conversion >95%. Pairs are rank ordered by oxygen transport capacity (R_{OC} , see the Experimental Section).

Oxidized phase	Reduced phase(s) ^{a)}	CH ₄ conv.	R_{OC}	K (sulfate) ^{b)}	Price ^{c)}	Temp. range ^{d)}	mp _{ox} ^{e)} [77]	mp _{red} ^{e)} [77]
Ga ₂ (SO ₄) ₃	Ga ₂ S ₃	0.99	0.45	4.1E-22	196	600–900	–	1090
CdSO ₄	CdS	0.99	0.31	7.9E-12	2.4	600–1100	1000	1750
Ag ₂ SO ₄	Ag ₂ S	0.99	0.21	7.0E-9	444	600–825	652	825
PbSO ₄	PbS	0.99	0.21	2.9E-11	1.65	600–1100	1087	1113
CrCuO ₂	Cr ₂ O ₃ , Cu	0.99	0.05	N/A	6.8	600–800	–	2329, 1084
YCuO ₂	Y ₂ O ₃ , Cu	0.99	0.04	N/A	40	900–1000	–	2439, 1084
YVO ₄	Y ₂ O ₃ , VO ₂	0.99	0.04	N/A	38	1000–1200	–	2439, 1967
SmCuO ₂	Sm ₂ O ₃ , Cu	0.99	0.03	N/A	39	600–1000	–	2269, 1084

^{a)}None of the listed redox pairs yield >1% side products; ^{b)}For sulfate/sulfide redox pairs, the equilibrium constant for the decomposition of the sulfate to the oxide and SO₂ (K) is shown at 1000 °C; ^{c)}Price is in \$ kg⁻¹; ^{d)}The temperature range indicates the temperatures within the CLC operating range where methane conversion is >95%, calculated at intervals of 100 °C, and where the reduced phase(s) are solid, All temperatures are in Celsius; ^{e)}mp_{ox} and mp_{red} are the melting points of the oxidized and reduced phases, respectively.

As such, some of the 1168 redox pairs that the Gibbs energy minimization approach predicts will yield conversions approaching 95% may still be experimentally viable OCs for CLC. Likewise, a fraction of the 152 promising redox pairs may in fact yield conversions below 95%. All 1320 thermodynamically viable redox pairs are available for download with their relevant calculated data in the Supporting Information, alongside the 16 560 nonviable redox pairs.

Our thermodynamic screening approach does not systematically consider melting points because experimental tabulation of this property is sparse, and its calculation is computationally demanding.^[56,81] As a result, some of the redox pairs predicted to be viable by our thermodynamic screening approach will not in fact be applicable for CLC because they include compounds that melt below CLC operating temperatures. **Table 1** reports a subset of the 152 high conversion redox pairs, including 3 of the 9 pairs that meet the R_{OC} and price cutoff and have not been previously studied for CLC (CdSO₄/CdS, PbSO₄/PbS, and CrCuO₂/Cr₂O₃+Cu). 5 of the other pairs are excluded due to having melting or decomposition temperatures near or below 600 °C (Bi₂(SO₄)₃/Bi₂S₃, CuSO₄/CuS, MnO₂/Mn₂O₃, Sb₂(SO₄)₃/Sb₂S₃, and ZnSO₄/ZnS),^[77] and the remaining pair from this set (Cu₂SO₅/Cu₂S) was removed due to possible degradation to the oxide, as discussed below. Despite their higher costs, additional pairs from the subset of 152 high conversion pairs have been included because of their high conversions and R_{OC} , including Ga₂(SO₄)₃/Ga₂S₃ and Ag₂SO₄/Ag₂S. Table 1 includes melting points where available. R_{OC} and price are also listed (see Experimental Section for details). Some of these materials may also be relevant for CL with oxygen uncoupling for solid fuel combustion or CL air separation, such as the perovskite SrNiO₃, which decomposes above 600 °C to yield SrNiO_{2.5} (mp = 1350 °C) and O₂.^[82] Multiple sulfate redox pairs are listed in Table 1 due to their high R_{OC} , high methane conversion and few or no side products. Although these sulfate redox pairs exhibit high figures of merit for CLC, they may be limited by partial degradation of the sulfide to the corresponding oxide during oxidation at higher temperatures, as is observed for CaSO₄/CaS above 950 °C.^[76] To determine the extent of this degradation, we have included equilibrium constants (K) in Table 1 for the sulfate decomposition reaction that yields SO₂ and the lowest energy

oxide(s). Further, we excluded any pairs with $K > 1 \times 10^{-8}$ at 1000 °C, including Cu₂SO₅/Cu₂S. These equilibrium constants are also provided for all of the sulfate/sulfide pairs in the downloadable dataset available in the Supporting Information.

2.4. Novel Chemical Looping Process for SO₂ Production

We also applied our thermodynamic screening approach to predict materials for a novel chemical looping process that we hypothesized can produce highly pure sulfur dioxide (SO₂), as shown in **Figure 5**. SO₂ is an essential industrial chemical because it is a precursor for sulfuric acid,^[83,84] a reducing agent

CHEMICAL LOOPING SULFUR OXIDATION

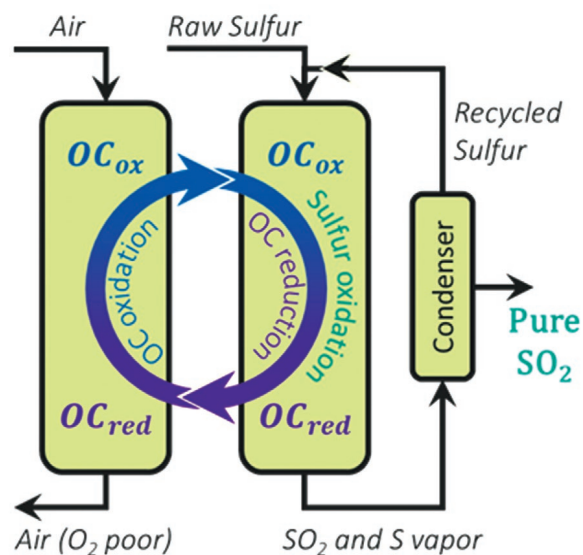
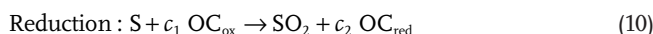


Figure 5. Proposed process for pure SO₂ production, envisioned in a circulating bed arrangement. An oxygen carrier, OC_{ox}, is used to oxidize sulfur to SO₂, concomitantly reducing the oxygen carrier. The reduced oxygen carrier, OC_{red}, is regenerated in a second reactor via aerobic oxidation. Any unreacted sulfur vapor is readily separated from the effluent via condensation and recycled.

for pulp and paper production,^[84] a dechlorinating agent in wastewater treatment,^[85] a food preservative (E220),^[86] an antioxidant for wine,^[87] a leachant for manganese ore,^[88] and used in the production of other sulfur-containing chemicals.^[65,89] The primary method for generating SO₂ for sulfuric acid production is via the aerobic combustion of sulfur (Equation (11)), which produces a dilute SO₂ stream that is ≈12% SO₂, 7% oxygen, and 79% nitrogen by volume.^[84] The substantial volume of inert N₂ dilutes this product stream, which dictates that gas flowrates and downstream process units must be proportionally larger and ultimately that energy intensive separations processes must be used to reduce the emission of unreacted SO₂ with the N₂-rich effluent.^[84] Some applications require concentrated (99.9%) liquid SO₂, whose production begins with the aerobic combustion of sulfur, followed by absorption–desorption, drying, and finally cryogenic condensation to concentrate the SO₂.^[65] These additional process steps to concentrate SO₂ are expensive and energy intensive.^[65] An efficient route to producing pure SO₂ using CL would therefore substantially decrease the capital cost, energy use, and SO₂ emissions of producing both concentrated liquid SO₂ and sulfuric acid, which would be significant considering that sulfuric acid is the world's most produced chemical by mass, with an annual production rate of 230 billion kg year⁻¹.^[66,84] Pure SO₂ produced via a CL process can be condensed and provided as liquid SO₂ or subsequently converted to sulfuric acid via the contact process using recently developed catalyst bed designs capable of processing high SO₂ content streams^[90,91]



Our descriptor-based screening approach enables a high-throughput screening strategy to discover thermodynamically viable redox pairs for the proposed chemical looping sulfur oxidation (CLSO) process. Sulfate/sulfide redox pairs were exclusively considered for this screening effort because metal oxides predominantly react with elemental sulfur at high temperatures to form sulfides and sulfates.^[92–94] Similar to our analysis of methane oxidation for CLC, $\Delta G_{\text{r,ox}}(T)$ (Equation (9)) was compared directly to the reaction free energy of the net reaction ($\Delta G_{\text{r,net}}(T)$, Equation (11)), which is again normalized to the reaction of 1 mole of O₂ with a reaction conversion of 90%. The Ellingham diagram depicted in **Figure 6** shows $\Delta G_{\text{r,ox}}(T)$ relative to $\Delta G_{\text{r,net}}(T)$ for 75 sulfate redox pairs and thus illustrates the thermodynamic viability of these pairs for CLSO. An operating range of 444–1150 °C was selected for this comparison because 444 °C is the boiling point of sulfur (at 1 atm),^[77] and 1150 °C is the conventional reactor temperature of a sulfur burning furnace.^[84]

The screening of CLSO redox materials based on their thermodynamic viability identifies three sulfate/sulfide redox pairs (PdSO₄/PdS, CuSO₄/CuS, and Ag₂SO₄/Ag₂S) as being thermodynamically viable OCs for CLSO within the defined operating range (444–1150 °C). All three of these pairs are within the MAE of ΔG_{r} but meet the condition that $\Delta G_{\text{r,red}}(T) < 0$. Of

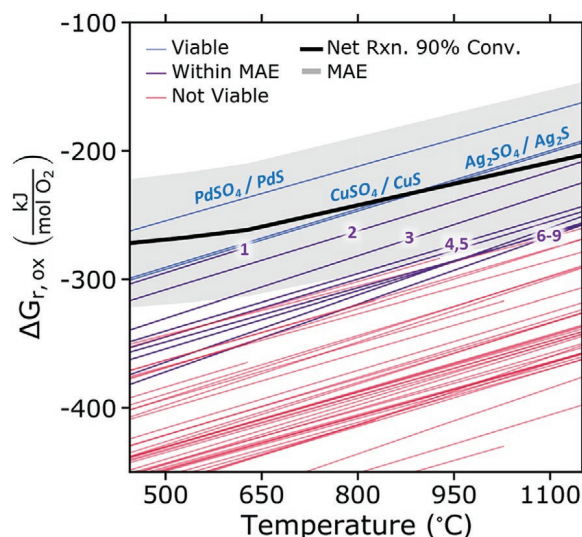


Figure 6. An Ellingham diagram for CLSO showing $\Delta G_{\text{r,ox}}(T)$ for 75 sulfate/sulfide redox pairs. All redox pairs are only shown in the temperature range where both the oxidized and reduced phases are stable. Thermodynamically viable redox pairs are those that meet the condition that $\Delta G_{\text{r,net}}(T) < \Delta G_{\text{r,ox}}(T)$ within the operating range of 444–1150 °C. Redox pairs 1–9 which lie within the MAE are (in order): W(SO₄)₂/WS₂, NiSO₄/NiS, Nb(SO₄)₂/NbS₂, PbSO₄/PbS, CoSO₄/CoS, CdSO₄/CdS, Ga₂(SO₄)₃/Ga₂S₃, Tl₂SO₄/Tl₂S, and Sb₂(SO₄)₃/Sb₂S₃.

these three, the redox pair CuSO₄/CuS is highly promising due to its thermodynamic viability and low cost. An additional 9 redox pairs (W(SO₄)₂/WS₂, NiSO₄/NiS, Nb(SO₄)₂/NbS₂, PbSO₄/PbS, CoSO₄/CoS, CdSO₄/CdS, Ga₂(SO₄)₃/Ga₂S₃, Tl₂SO₄/Tl₂S, and Sb₂(SO₄)₃/Sb₂S₃) are identified within the MAE of ΔG_{r} that meet the condition that $\Delta G_{\text{r,red}}(T) < \text{MAE}(T)$. Because $\Delta G_{\text{r,red}}(T)$ of these pairs lies within the MAE of the threshold for thermodynamic viability, they could be experimentally viable for CLSO and are therefore included in the following screening. We next performed a Gibbs energy minimization for both the oxidation and reduction reactions for all 12 of the redox pairs to determine the equilibrium reaction conversions with consideration of the possible competing reactions. For the reduction reaction, the maximum sulfur conversion and predicted side products are tabulated alongside relevant material properties, where available, for each redox pair in **Table 2**. To determine whether partial degradation to the oxide occurs during oxidation of the sulfide, we calculated the equilibrium constants, *K*, for these reactions. All 12 oxidation reactions exhibit >99.9% conversion of the sulfide to the corresponding sulfate and $K < 1 \times 10^{-17}$ at 600 °C except W(SO₄)₂ and CuSO₄ which are 1.6×10^{-13} and 8.0×10^{-6} , respectively. Additionally, any minor degradation of the sulfide to the oxide during oxidation would be rectified when reacting the oxide with sulfur vapors during the reduction reaction that regenerates the sulfide.

Of the 12 candidates reported in **Table 2**, PdSO₄, Tl₂SO₄, Ag₂SO₄, and Ga₂(SO₄)₃ are likely too expensive to be considered for industrial applications.^[78] Furthermore, Sb₂(SO₄)₃ is experimentally observed to be thermodynamically unstable.^[77] Of the remaining 7 candidates, the sulfates of W, Nb, and Ni demonstrate the highest conversions with minimal side-product formation, making them the most promising candidate OCs for

Table 2. 12 viable and nearly viable sulfate redox pairs for CLSO listed in order of decreasing viability (i.e., increasing $\Delta G_{r,\text{red}}$).

Oxidized phase	Reduced phase(s)	Sulfur conv.	R_{OC}	Side prod.	Price ^{a)}	Temp. range ^{b)}	$\text{mp}_{\text{ox}}^{\text{c)[77]}$	$\text{mp}_{\text{red}}^{\text{c)[77]}$
PdSO ₄	PdS	0.99	0.32	PdS ₂	9300	700–1150	–	–
Ag ₂ SO ₄	Ag ₂ S	0.97	0.21	None	440	600–825	652	825
CuSO ₄	CuS	0.66	0.40	CuS ₂	3.1	450–507	560 (d) ^{d)}	507 (d)
W(SO ₄) ₂	WS ₂	0.97	0.34	WO ₃	0.1	550–750	–	1250 (d)
NiSO ₄	NiS	0.81	0.41	NiS ₂ , Ni ₃ S ₄	8.3	450–946	840 (d)	946
Nb(SO ₄) ₂	NbS ₂	0.70	0.45	Nb ₂ O ₅ , NbS ₃	5.0	600–1150	–	–
PbSO ₄	PbS	0.59	0.21	PbS ₂ O ₃	1.7	550–1113	1087	1113
CoSO ₄	CoS	0.58	0.41	CoS ₂	18	650–1150	>700	1182
CdSO ₄	CdS	0.68	0.31	CdS ₂	2.4	850–1150	1000	1750
Ga ₂ (SO ₄) ₃	Ga ₂ S ₃	0.49	0.45	None	200	950–1090	–	1090
Tl ₂ SO ₄	Tl ₂ S	–	0.13	–	4800	–	632	448
Sb ₂ (SO ₄) ₃	Sb ₂ S ₃	0.00	0.36	None	4.0	450–550	(d)	550

^{a)}Price is in \$ kg⁻¹; ^{b)}The temperature range indicates where the tabulated corresponding sulfur conversion is achieved, and the reduced phase(s) is stable and solid. All temperatures are in Celsius; ^{c)} mp_{ox} and mp_{red} are the melting points of the oxidized and reduced phases, respectively; ^{d)}(d) indicates that the material decomposes at the indicated temperature.

CLSO. The formation of oxide side products (e.g., WO₃ and Nb₂O₅) during sulfate reduction does not hinder the recyclability of the OCs because these side products are also inherently oxygen carriers. Gibbs energy minimization indicates that both WO₃ and Nb₂O₅ react with sulfur vapor to produce the corresponding sulfides and SO₂. All of the candidates included in Table 2 exhibit a high oxygen transport capacity.

Previous experimental studies on the reduction of sulfates and oxidation of sulfides corroborate several of our material predictions. The sulfates and oxides of Cu and Ni have been demonstrated to spontaneously react with sulfur vapor to form the corresponding metal sulfide under low-oxygen conditions,^[95–97] even at lower temperatures (450 °C for Ni), agreeing with our predictions from $\Delta G_{r,\text{red}}$ indicating that the reaction of CuSO₄ and NiSO₄ with sulfur is spontaneous (or nearly so). Additionally, the sulfides of Ni,^[98,99] Cu,^[100] and Co^[100,101] have been observed to spontaneously oxidize to a mixture of the sulfide, sulfate, and oxide phases with minimal or no SO₂ release when properly controlled. This agrees with our calculations that NiS, CuS, and CoS spontaneously react with air to form the corresponding sulfate without substantial side-product formation. The oxidation of nickel sulfide particles occurs in stages, with the initial stage of the reaction forming a dense nickel oxide layer as Ni atoms migrate to the surface of the particle.^[98] This initial oxidation stage proceeds with little evolution of SO₂. The sulfides of Cu and Co react in an analogous manner with optimal oxidation occurring near 450 °C.^[100,101] Reactor conditions should be properly regulated to minimize the production of SO₂ during aerobic oxidation of the sulfide; however, experiments with fluidized bed reactors have demonstrated that this is achievable for sulfate roasting applications.^[100,102] Although no study has previously investigated both the oxidation and reduction reactions considered for CLSO, experimental results support our contention that the constituent oxidation and reduction reactions of CLSO can be individually accomplished with a high degree of control for the sulfate/sulfide OCs based on Ni and Cu.^[95–100]

3. Conclusion

High-throughput materials screening is a promising route to accelerate the discovery of active materials for chemical looping processes. Here, we demonstrated that a high-throughput thermodynamic screening approach based on our Gibbs energy descriptor $G^\delta(T)$ can be broadly applied to chemical looping processes that operate at or near equilibrium with similar accuracy across a wide range of materials. We provide an estimate for the mean absolute error in $\Delta G_r(T)$ using this approach, which ranges from 43 kJ mol O₂⁻¹ at 0 K, due to errors in the DFT calculated reaction enthalpies, to 62 kJ mol O₂⁻¹ at 1800 K, due to the additional error contributed by the $G^\delta(T)$ descriptor in predicting high-temperature contributions to the free energy. These errors will decrease as ab initio databases increase in accuracy and the 0 K error decreases. For CLC, our screening method properly classified 100% (17/17) of the experimentally studied redox materials by their thermodynamic viability for this process. Moreover, we leveraged this approach to analyze unstudied redox materials for CLC and identified over 1300 viable redox pairs, 152 of which are predicted to exhibit reaction conversions of methane >95% with minimal side product formation, increasing the number of known materials that meet these constraints by an order of magnitude. Furthermore, a number of sulfate materials (e.g., CdSO₄, PbSO₄, etc.) are included in this set that not only exhibit high reaction conversion and minimal side-product formation, but which are also inexpensive and exhibit exemplary oxygen transport capacities, making them intriguing candidates for CLC.

Finally, we further demonstrated the ability of our thermodynamic screening approach by applying it to a novel chemical looping process to oxidize raw sulfur to pure SO₂. This process could provide a considerably more energy efficient and lower emission route to sulfuric acid. Application of our screening approach revealed that 12 possible sulfate/sulfide redox pairs are thermodynamically viable for this process. 7 of these pairs involve low cost materials with calculated reaction conversions >50% and high oxygen transport capacities. One of these

materials, $W(SO_4)_2$, is calculated to yield 97% conversion of sulfur to SO_2 . Two others, $NiSO_4$ and $CuSO_4$, are corroborated by experimental studies of their individual sulfide oxidation and sulfate reduction reactions constituting the CLSO process and are predicted to achieve sulfur oxidation conversions of 81% and 66%, respectively. As the field of chemical looping continues to grow, our screening approach provides a platform for rapid materials discovery to accelerate innovation across a wide range of chemical looping chemistries capable of increasing energy efficiency, leveraging renewable energy sources, facilitating chemical conversions, and decreasing undesirable emissions in many sectors of the chemical industry.

4. Experimental Section

Formation enthalpies (ΔH_f) and atomic densities of materials were obtained from the Materials Project (MP) database, which currently contains calculated properties for over 120 000 inorganic crystal structures.^[103] A subset of materials that are consistent with the known classes of active materials for CLC, specifically, binary oxides, ternary oxides, and sulfates, was selected. Sulfides were included as possible reduction products. The MP database contained 13 763 compounds from this subset and their respective 0 K properties. Similarly, for chemical looping sulfur oxidation sulfates and sulfides were investigated; MP contained 1238 compounds in this subset. Compounds containing radioactive elements were not considered. $\Delta G_f(T)$ for all entries in the MP database were calculated for the temperature range of 300–1800 K at intervals of 100 K using the statistically learned physical descriptor $G^\delta(T)$.^[60] $\Delta G_f(T)$ for nonsolids (e.g., CH_4 , H_2O , CO_2 , SO_2 , etc.) at 1 atm were obtained from the NIST JANAF thermochemical database.^[56] Decomposition energies, $\Delta G_d(T)$, were calculated over the temperature range of 300–1800 K using $\Delta G_f(T)$ and the convex hull construction. Materials with $\Delta G_d(T) < 0$ are stable relative to all competing phases at their corresponding compositions.^[67] The convex hull method is described in Section S3 (Supporting Information), and ref. [67]. $\Delta G_d(T)$ does not indicate whether a compound will melt or boil at a particular temperature.

Redox pairs were identified from the subset of stable materials. Each redox pair was comprised of a single oxidized compound (M_{ox}), and either one or two reduced materials (M_{red}). Elemental phases were considered for the reduced material(s). Redox pairs were only investigated for thermodynamic viability at temperatures at which all constituent compounds are stable. 17 880 redox pairs meet this constraint for CLC. Stoichiometric coefficients for the subreactions (i.e., oxidation and reduction) of the redox pairs were normalized to maintain molar conservation with 1 mol of O_2 liberated from M_{ox} during the reduction reaction (Equation (2)), enabling the reaction energies of different redox pairs to be directly compared.

A thermodynamically viable redox pair is defined as one which undergoes both the oxidation and reduction reactions (Equations (1) and (2)) spontaneously ($\Delta G_r(T) < 0$). Temperature-dependent Gibbs energies of reaction, $\Delta G_r(T)$, are calculated as the differences in free energy between the stoichiometrically weighted $\Delta G_f(T)$ of the products and reactants. For reactions involving gaseous species, an ideal gas correction term was included to account for the partial pressure of the gas: $\Delta G_f(T) = \Delta G_f^\circ(T) + RT \ln(P_x)$, where ΔG_f° is the Gibbs formation energy at standard state pressure (1 atm) and x is the gaseous species of interest. Partial pressures are calculated at 90% conversion at a total pressure of 1 atm throughout this work. Other reaction pressures could be studied using this approach but were not considered here.

The errors in $\Delta G_r(T)$ relative to experiment were determined to arise predominantly from errors in the DFT-calculated reaction enthalpy, ΔH_r , and to a lesser extent, the descriptor-calculated temperature-dependent contribution to $\Delta G_f(T)$. Additional errors in ΔH_r arise for redox pairs that contain the magnetic elements Cr, Mn, Fe, Co, and Ni because

antiferromagnetism is not systematically considered in Materials Project calculations.^[103,104] To mitigate this additional error, ΔH_f for binary oxides (listed in Table S5, Supporting Information) containing these magnetic elements were calculated. One ferromagnetic and ≈ 8 antiferromagnetic supercells were enumerated for each of the oxides containing these elements using MP calculation standards in order to determine magnetic ground states, and thus more accurate ΔH_f , while maintaining consistency with the MP database. Atomic structures and total energy calculations were performed using the projector augmented-wave method within the Vienna Ab initio Simulation Package (VASP).^[105] The Perdew–Burke–Ernzerhof (PBE) generalized gradient approximation (GGA) functional was used with a plane-wave energy cutoff of 520 eV.^[106] A Γ -centered Monkhorst–Pack k-point grid was employed with a k-point mesh density of 1000/(atoms in the unit cell). A Hubbard +U correction was included using the Dudarev method for calculations of oxides and an MP correctional term was applied to these calculations to maintain MP compatibility.^[103,107]

The equilibrium product distribution at any temperature was obtained by Gibbs energy minimization, which is described in detail in Section S6 (Supporting Information). Equilibrium conversions were calculated as the ratio between the moles of the desired product (i.e., the value-added product) at equilibrium and the theoretical maximum number of moles of the desired product. Equilibrium constants, K , were calculated using $K = e^{-\Delta G_r/RT}$, where T is the temperature in Kelvin and R is the ideal gas constant. Thermodynamically viable redox pairs were ranked based on their calculated oxygen transport capacity, R_{OC} , which are quantified as

$$R_{OC} = \frac{m_o - m_r}{m_o}$$

where m_o is the mass of the oxidized material and m_r is the mass of the reduced material.^[23,68] As R_{OC} decreases, the circulation rate of solids in the CL process must increase to maintain a constant conversion rate.^[23] Thus, a higher R_{OC} is desirable. Prices of elements were obtained from the United States Geological Survey.^[78] Prices of the OC materials were approximated from the price of the constituent metals (oxygen and sulfur are excluded) necessary to produce 1 kg of material.

Supporting Information

Supporting Information is available from the Wiley Online Library or from the author.

Acknowledgements

N.R.S. was supported by a U.S. Department of Education Graduate Assistance in Areas of National Need Fellowship under the Materials for Energy Conversion and Sustainability program. C.B.M., A.M.H., and N.R.S. were also supported by the U.S. National Science Foundation (Awards CBET-1806079 and CHE-1800592) for the machine-learned descriptor application and chemical looping process discovery work, respectively, along with the U.S. Department of Energy, Fuel Cell Technologies Office (Award DEEE0008088) for performing the high-throughput calculations and computational materials discovery.

Conflict of Interest

The authors declare no conflict of interest.

Author Contributions

N.R.S. performed all calculations, analyzed the results, conceived of the CLSO process, and drafted the manuscript. C.J.B., C.B.M., and A.M.H. conceived of the project, designed the initial approach, provided essential guidance on the project and analysis, and assisted in writing and revising the manuscript. All of the authors reviewed the manuscript.

Keywords

chemical looping, high-throughput screening, machine learning, redox catalysis

Received: February 21, 2020

Revised: April 16, 2020

Published online:

- [1] X. Zhu, F. Donat, Q. Imtiaz, C. R. Müller, F. Li, *Energy Environ. Sci.* **2020**, *14*, 112.
- [2] Y. Chen, X. Zhu, K. Li, Y. Wei, Y. Zheng, H. Wang, *ACS Sustainable Chem. Eng.* **2019**, *7*, 15452.
- [3] C. L. Muhich, B. W. Evanko, K. C. Weston, P. Lichty, X. Liang, J. Martinek, C. B. Musgrave, A. W. Weimer, *Science* **2013**, *341*, 540.
- [4] S. Tian, F. Yan, Z. Zhang, J. Jiang, *Sci. Adv.* **2019**, *5*, eaav5077.
- [5] R. Michalsky, A. M. Avram, B. A. Peterson, P. H. Pfromm, A. A. Peterson, *Chem. Sci.* **2015**, *6*, 3965.
- [6] W. C. Chueh, M. Abbott, D. Scipio, S. M. Haile, *Science* **2010**, *330*, 1797.
- [7] C. J. Bartel, J. R. Rumpitz, A. W. Weimer, A. M. Holder, C. B. Musgrave, *ACS Appl. Mater. Interfaces* **2019**, *11*, 24850.
- [8] Z. Sun, L. Zeng, C. K. Russell, S. Assabumrungrat, S. Chen, L. Duan, W. Xiang, J. Gong, *ACS Sustainable Chem. Eng.* **2019**, *7*, 2558.
- [9] D. F. Swearer, N. R. Knowles, H. O. Everitt, N. J. Halas, *ACS Energy Lett.* **2019**, *4*, 1505.
- [10] C. L. Muhich, B. D. Ehrhart, V. A. Witte, S. L. Miller, E. N. Coker, C. B. Musgrave, A. W. Weimer, *Energy Environ. Sci.* **2015**, *8*, 3687.
- [11] R. H. Wentorf, R. E. Hanneman, *Science* **1974**, *185*, 311.
- [12] W. Gao, J. Guo, P. Wang, Q. Wang, F. Chang, Q. Pei, W. Zhang, L. Liu, P. Chen, *Nat. Energy* **2018**, *3*, 1067.
- [13] O. Planas, F. Wang, M. Leutzsch, J. Cornella, *Science* **2020**, *367*, 313.
- [14] Y. Gao, L. M. Neal, F. Li, *ACS Catal.* **2016**, *6*, 7293.
- [15] C. Brady, B. Murphy, B. Xu, *ACS Catal.* **2017**, *7*, 3924.
- [16] J. Huang, W. Liu, Y. Yang, B. Liu, *ACS Catal.* **2018**, *8*, 1748.
- [17] Y. Gao, L. Neal, D. Ding, W. Wu, C. Baroi, A. M. Gaffney, F. Li, *ACS Catal.* **2019**, *9*, 8592.
- [18] Q. Shen, F. Huang, M. Tian, Y. Zhu, J. Wang, X. Wang, *ACS Catal.* **2019**, *9*, 722.
- [19] Y. Liu, L. Qin, Z. Cheng, J. W. Goetze, F. Kong, J. A. Fan, L.-S. Fan, *Nat. Commun.* **2019**, *10*, 5503.
- [20] J. Zhang, V. Haribal, F. Li, *Sci. Adv.* **2017**, *3*, e1701184.
- [21] X. Zhao, H. Zhou, V. S. Sikarwar, M. Zhao, A. A. Park, P. S. Fennell, L. Shenf, L.-S. Fan, *Energy Environ. Sci.* **2017**, *10*, 1885.
- [22] L.-S. Fan, L. Zeng, W. Wang, S. Luo, *Energy Environ. Sci.* **2012**, *5*, 7254.
- [23] J. Adanez, A. Abad, F. Garcia-Labiano, P. Gayan, L. F. de Diego, *Prog. Energy Combust. Sci.* **2012**, *38*, 215.
- [24] X. Zhu, K. Li, L. Neal, F. Li, *ACS Catal.* **2018**, *8*, 8213.
- [25] N. S. Yüzbası, A. Armutlulu, P. M. Abdala, C. R. Müller, *ACS Appl. Mater. Interfaces* **2018**, *10*, 37994.
- [26] J. M. Valverde, S. Medina, *ACS Sustainable Chem. Eng.* **2016**, *4*, 7090.
- [27] B. Moghtaderi, *Energy Fuels* **2012**, *26*, 15.
- [28] S. Bhavsar, M. Najera, R. Solunke, G. Veser, *Catal. Today* **2014**, *228*, 96.
- [29] L.-S. Fan, L. Zeng, S. Luo, *AIChE J.* **2015**, *61*, 2.
- [30] A. Lyngfelt, C. Linderholm, *Energy Procedia* **2017**, *114*, 371.
- [31] M. Ishida, D. Zheng, T. Akehata, *Energy* **1987**, *12*, 147.
- [32] B. Chen, Z. Liao, J. Wang, H. Yu, Y. Yang, *Int. J. Hydrogen Energy* **2012**, *37*, 3191.
- [33] C. L. Muhich, B. D. Ehrhart, I. Al-Shankiti, B. J. Ward, C. B. Musgrave, A. W. Weimer, *Wiley Interdiscip. Rev.: Energy Environ.* **2016**, *5*, 261.
- [34] M. Ishida, H. Jin, *Energy* **1994**, *19*, 415.
- [35] M. Tang, L. Xu, M. Fan, *Appl. Energy* **2015**, *151*, 143.
- [36] R. H. Wentorf, R. E. Hanneman, *Science* **1974**, *185*, 311.
- [37] S. Hurst, *J. Am. Oil Chem. Soc.* **1939**, *16*, 29.
- [38] B. Moghtaderi, *Energy Fuels* **2010**, *24*, 190.
- [39] J. Dou, E. Krzystowczyk, A. Mishra, X. Liu, F. Li, *ACS Sustainable Chem. Eng.* **2018**, *6*, 15528.
- [40] G. E. Keller, M. M. Bhasin, *J. Catal.* **1982**, *73*, 9.
- [41] C. A. Jones, J. J. Leonard, J. A. Sofranko, *J. Catal.* **1987**, *103*, 311.
- [42] M. E. Gálvez, M. Halmann, A. Steinfeld, *Ind. Eng. Chem. Res.* **2007**, *46*, 2042.
- [43] R. Porrazzo, G. White, R. Ocone, *Faraday Discuss.* **2016**, *192*, 437.
- [44] C. Zhou, K. Shah, B. Moghtaderi, *Energy Fuels* **2015**, *29*, 2074.
- [45] D. Xiang, Y. Zhou, *Appl. Energy* **2018**, *229*, 1024.
- [46] S. C. Bayham, H. R. Kim, D. Wang, A. Tong, L. Zeng, O. McGiveron, M. V. Kathe, E. Chung, W. Wang, A. Wang, A. Majumder, L.-S. Fan, *Energy Fuels* **2013**, *27*, 1347.
- [47] A. Tong, D. Sridhar, Z. Sun, H. R. Kim, L. Zeng, F. Wang, D. Wang, M. V. Kathe, S. Luo, Y. Sun, L.-S. Fan, *Fuel* **2013**, *103*, 495.
- [48] R. M. Contractor, *Chem. Eng. Sci.* **1999**, *54*, 5627.
- [49] M. P. Dudukovic, *Science* **2009**, *325*, 698.
- [50] S. Lin, M. Harada, Y. Suzuki, H. Hatano, *Energy Convers. Manage.* **2005**, *46*, 869.
- [51] C. A. Jones, J. J. Leonard, J. A. Sofranko, *Energy Fuels* **1987**, *1*, 12.
- [52] E. Jendral, T. Mattisson, A. Lyngfelt, *Chem. Eng. Res. Des.* **2006**, *84*, 795.
- [53] K. Shah, B. Moghtaderi, T. Wall, *Energy Fuels* **2012**, *26*, 2038.
- [54] S. K. Thengane, A. Hoadley, S. Bhattacharya, S. Mitra, S. Bandyopadhyay, *Chem. Eng. Res. Des.* **2018**, *132*, 252.
- [55] K. Wang, Q. Yu, Q. Qin, *J. Therm. Anal. Calorim.* **2013**, *112*, 747.
- [56] M. W. Chase, *NIST-JANAF Thermochemical Tables*, 4th ed., American Institute of Physics, College Park, MD **1998**.
- [57] P. Carrier, R. Wentzcovitch, J. Tsuchiya, *Phys. Rev. B* **2007**, *76*, 189901.
- [58] A. Togo, I. Tanaka, *Scr. Mater.* **2015**, *108*, 1.
- [59] L. F. Huang, X. Z. Lu, E. Tennesen, J. M. Rondinelli, *Comput. Mater. Sci.* **2016**, *120*, 84.
- [60] C. J. Bartel, S. L. Millican, A. M. Deml, J. R. Rumpitz, W. Tumas, A. W. Weimer, S. Lany, V. Stevanović, C. B. Musgrave, A. M. Holder, *Nat. Commun.* **2018**, *9*, 4168.
- [61] H. A. Alalwan, S. E. Mason, V. H. Grassian, D. M. Cwiertny, *Energy Fuels* **2018**, *32*, 7959.
- [62] Q. Zafar, T. Mattisson, B. Gevert, *Energy Fuels* **2006**, *20*, 34.
- [63] G. Azimi, H. Leion, T. Mattisson, M. Rydén, F. Sniijkers, A. Lyngfelt, *Ind. Eng. Chem. Res.* **2014**, *53*, 10358.
- [64] J. Adánez, A. Abad, T. Mendiara, P. Gayán, L. F. de Diego, F. García-Labiano, *Prog. Energy Combust. Sci.* **2018**, *65*, 6.
- [65] N. G. Ashar, *Advances in Sulphonation Techniques Liquid Sulphur Dioxide as a Solvent of Sulfur Trioxide*, Springer, Berlin, Germany **2016**.
- [66] L. Apodaca, *Mineral Commodity Summaries 2018: Sulfur*, U.S. Geological Survey, Reston, VA **2018**.
- [67] C. J. Bartel, A. W. Weimer, S. Lany, C. B. Musgrave, A. M. Holder, *npj Comput. Mater.* **2019**, *5*, 4.
- [68] K. Lejaeghere, V. Van Speybroeck, G. Van Oost, S. Cottenier, *Crit. Rev. Solid State Mater. Sci.* **2014**, *39*, 1.
- [69] P. Cho, T. Mattisson, A. Lyngfelt, *Fuel* **2004**, *83*, 1215.
- [70] L. F. de Diego, F. García-Labiano, J. Adánez, P. Gayán, A. Abad, B. M. Corbella, J. M. Palacios, *Fuel* **2004**, *83*, 1749.
- [71] E. R. Stobbe, B. A. De Boer, J. W. Geus, *Catal. Today* **1999**, *47*, 161.
- [72] Q. Song, R. Xiao, Z. Deng, L. Shen, M. Zhang, *Energy Convers. Manage.* **2008**, *49*, 3178.
- [73] L. Shen, M. Zheng, J. Xiao, R. Xiao, *Combust. Flame* **2008**, *154*, 489.

- [74] H. A. Alalwan, D. M. Cwiertny, V. H. Grassian, *Chem. Eng. J.* **2017**, 319, 279.
- [75] A. Siewiorek, K. Svoboda, J. Rogut, *Chem. Pap.* **2007**, 61, 110.
- [76] H. Tian, Q. Guo, J. Chang, *Energy Fuels* **2008**, 22, 3915.
- [77] M. W. Haynes, *CRC Handbook of Chemistry and Physics*, CRC Press, Boca Raton, FL **2015**.
- [78] USGS, *Metal Prices in the United States through 2010*, U.S. Geological Survey, Reston, VA **2012**.
- [79] K. Fukuda, I. Nakai, Y. Ebina, R. Ma, T. Sasaki, *Inorg. Chem.* **2007**, 46, 4787.
- [80] R. C. Rau, *Acta Crystallogr.* **1966**, 20, 716.
- [81] L.-F. Zhu, B. Grabowski, J. Neugebauer, *Phys. Rev. B* **2017**, 96, 224202.
- [82] M. Zinkevich, *J. Solid State Chem.* **2005**, 178, 2818.
- [83] J. G. Speight, *Environmental Inorganic Chemistry for Engineers*, Elsevier, Amsterdam, Netherlands **2017**.
- [84] M. J. King, W. G. Davenport, M. S. Moats, *Sulfuric Acid Manufacture: Analysis, Control and Optimization*, Elsevier, Amsterdam, Netherlands **2013**.
- [85] R. L. Droste, R. L. Gehr, *Theory and Practice of Water and Wastewater Treatment*, Wiley, Hoboken, NJ, USA **2019**.
- [86] B. L. Wedzicha, *Chemistry of Sulphur Dioxide in Foods*, Elsevier, Amsterdam, Netherlands **1984**.
- [87] R. F. Guerrero, E. Cantos-Villar, *Trends Food Sci. Technol.* **2015**, 42, 27.
- [88] C. Abbruzzese, *Hydrometallurgy* **1990**, 25, 85.
- [89] A. Deeming, E. Emmett, C. Richards-Taylor, M. Willis, *Synthesis* **2014**, 46, 2701.
- [90] T. Weber, presented at Brazilian Congress of Sulfuric Acid, Brazil, October **2015**.
- [91] K. Daum, *J. South Afr. Inst. Min. Metall.* **2009**, 109, 469.
- [92] T. Luo, J. M. Vohs, R. J. Gorte, *J. Catal.* **2002**, 210, 397.
- [93] X. Wu, H. R. Lee, S. Liu, D. Weng, *J. Rare Earths* **2012**, 30, 659.
- [94] C. N. Alpers, J. L. Jambor, D. Nordstrom, *Rev. Mineral. Geochem.* **2000**, 40, 351.
- [95] R. Ma, J. Stegemeier, C. Levard, J. G. Dale, C. W. Noack, T. Yang, G. E. Brown Jr., G. V. Lowry, *Environ. Sci.: Nano* **2014**, 1, 347.
- [96] H. Siyu, L. Xinyu, L. Qingyu, M. Mianwu, L. Tengfa, J. Zhiliang, *Solid State Sci.* **2011**, 13, 1375.
- [97] F. T. Eggertsen, R. M. Rogers, *Anal. Chem.* **1950**, 22, 924.
- [98] Z. Asaki, K. Hajika, T. Tanabe, Y. Kondo, *Metall. Trans. B* **1984**, 15, 127.
- [99] J. G. Dunn, C. E. Kelly, *J. Therm. Anal.* **1977**, 12, 43.
- [100] F. J. Thoumsin, R. Coussement, *JOM* **1964**, 16, 831.
- [101] Z. Asaki, M. Nitta, T. Tanabe, Y. Kondo, *Metall. Trans. B* **1986**, 17, 367.
- [102] L. F. Theys, L. V. Lee, *JOM* **1958**, 10, 134.
- [103] A. Jain, S. P. Ong, G. Hautier, W. Chen, W. D. Richards, S. Dacek, S. Cholia, D. Gunter, D. Skinner, G. Ceder, K. A. Persson, *APL Mater.* **2013**, 1, 011002.
- [104] G. Kresse, J. Furthmüller, *Phys. Rev. B* **1996**, 54, 115.
- [105] J. P. Perdew, K. Burke, M. Ernzerhof, *Phys. Rev. Lett.* **1996**, 77, 3865.
- [106] S. L. Dudarev, G. A. Botton, S. Y. Savrasov, C. J. Humphreys, A. P. Sutton, *Phys. Rev. B* **1998**, 57, 1505.
- [107] J. Adánez, L. F. De Diego, F. García-Labiano, P. Gayá, A. Abad, J. M. Palacios, *Energy Fuels* **2004**, 18, 371.